Controlled blueshift of the resonant wavelength in porous silicon microcavities using ion irradiation

D. Mangaiyarkarasi, M. B. H. Breese,[a] and Y. S. Ow
Centre for Ion Beam Applications, Department of Physics, National University of Singapore, Singapore 117542

C. Vijila
Institute of Materials Research Engineering, 3 Research Link, Singapore 117602

High-energy focused proton beam irradiation has been used to controllably blueshift the resonant wavelength of porous silicon microcavities in heavily doped *p*-type wafers. Irradiation results in an increased resistivity, hence a locally reduced rate of anodization. Irradiated regions are consequently thinner and of a higher refractive index than unirradiated regions, and the microcavity blueshift arises from a net reduction in the optical thickness of each porous layer. Using this process wafers are patterned on a micrometer lateral scale with microcavities tuned to different resonant wavelengths, giving rise to high-resolution full-color reflection images over the full visible spectrum. © *2006 American Institute of Physics*. [DOI: 10.1063/1.2219989]

The optical properties of porous silicon (PSi) have been intensively studied for many years[1–3] and it has found applications in many areas such as silicon photonics and integrated silicon opto- and microelectronics. While the photoluminescence (PL) from PSi is too broad and faint for many light-emitting applications its properties can be greatly improved by placing it in a Fabry-Pérot microcavity with dimensions comparable to the optical emission wavelength. One-dimensional photonic structures based on alternating high and low porosity PSi layers have found applications as dielectric mirrors in the form of distributed Bragg reflectors,[4] microcavities (MCs),[5,6] and waveguides,[7] and may have a future role as optical interconnects and switches in future microelectronics technology.[8,9]

PSi exhibits optical properties consistent with a single effective refractive index *n*, despite its nanoscale structural inhomogeneity. Within an effective medium approximation, *n* of PSi is lower than for bulk silicon;[6] it is inversely proportional to the etch current density *J* used for anodization, so higher *J* results in lower *n*. A distributed Bragg reflector selectively reflects a band of incident wavelengths of width $\Delta\lambda$ and is formed in PSi by periodically lowering and raising *J*, resulting in a sequence of porous layers with alternating high and low refractive index. Each porous layer of thickness *d* and refractive index *n* has an optical thickness *nd* equal to $\lambda/4$, where λ is the central wavelength of the resonant reflected peak. Highly doped *p*-type silicon ($\sim 0.01 \ \Omega$ cm) is commonly used to fabricate such PSi based photonic structures because a wide range of *n* can be achieved by varying *J*,[3,6,10,11] though moderately doped silicon ($1-10 \ \Omega$ cm) has also been used.[12,13]

MCs are formed by separating two such distributed Bragg reflectors with a PSi spacer layer of optical thickness $\lambda/2$ or any multiple. The central layer breaks the repetitive sequence and results in transmission rather than reflection of a narrow band of wavelengths centered on λ. MCs act as highly selective wavelength filters and good quality MCs have been grown with emission properties superior to bulk

PSi.[6,14,15] The resultant narrowing, enhancement, and directionality of the resonant PL (Refs. 11 and 12) and electroluminescence wavelengths[5,16] of such structures has been reported. Subnanometer transmitted linewidths have been produced by anodization at $-22 \ °$C (Ref. 17) and in freestanding PSi MCs in the standard window of fiber optic attenuation of 1.55 μm.[18] Controlled wavelength PL and electroluminescence were obtained from MCs by varying the porosity of the central PSi layer.[19] Electrically tunable active mirrors were produced by filling the porous structure with liquid crystal molecules.[20] Application of a small voltage produced a shift in the location of the linewidth, and so a change in reflectivity of a particular wavelength.

Focused MeV ion beams in a nuclear microprobe[21] have been used to fabricate patterned PSi layers with micron lateral resolution.[22–25] 2 MeV protons lose energy as they penetrate silicon and come to rest at a well-defined range of $\sim 50 \ \mu$m. The stopping process damages the silicon lattice by producing additional defects which locally reduce the concentration of free charge carriers, i.e., increase the resistivity.[25] Ion irradiation was used to increase the PL intensity emitted from 0.02 Ω cm *p*-type silicon[22] and controllably redshift the PL of $1-10 \ \Omega$ cm *p*-type silicon. The latter was attributed to the irradiated layers being slightly less porous, exhibiting a smaller widening of the band gap and reduced quantum confinement effects associated with larger nanocrystallite sizes.

Here the ability of 2 MeV proton beam irradiation to controllably alter the reflected peak central wavelength and width of PSi MCs produced in 0.02 Ω cm *p*-type wafers is studied. In each case, wafers were first proton irradiated with a beam spot size of ~ 100 nm and then electrochemically etched at room temperature in a solution of HF (48%): water:ethanol in the ratio of 1:1:2. After etching, the sample was briefly washed in ethanol and dried in air.

Figure 1 shows scanning electron micrographs of a sample in which lines were irradiated with different fluences in a $1 \times 1 \ $cm^2 wafer. The wafer was etched with *J* alternating between 10 and 100 mA/cm^2 for 4 s per layer, with a total of 15 bilayers formed, then cleaved perpendicular to the

[a]FAX: +65 6777 6126; electronic mail: phymbhb@nus.edu.sg
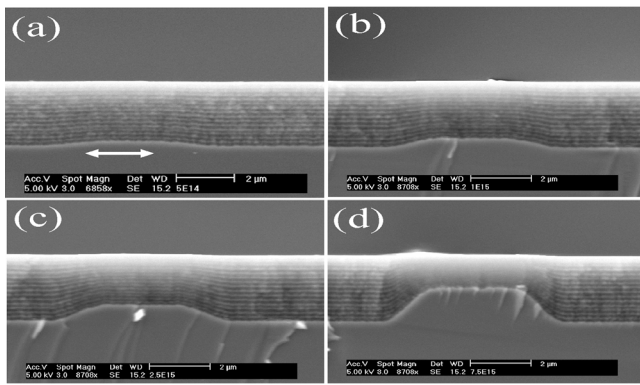
FIG. 1. Scanning electron micrographs of lines irradiated with fluences of (a) $5 \times 10^{14}/cm^2$, (b) $1 \times 10^{15}/cm^2$, (c) $2.5 \times 10^{15}/cm^2$, and (d) 7.5 $\times 10^{15}/cm^2$. The lines were 2 mm long and 2 μm wide. The line is arrowed in (a) where it is least obvious.

line direction for cross-section imaging. The etched layers appear with light/dark contrast, with high porosity (low n) regions appearing darker. The etching rate is progressively slowed by a larger fluence, resulting in thinner porous layers. Figure 1 also provides interesting observation of the evolution of the etching process across an irradiated boundary, since each change of J is clearly delineated. The irradiated region becomes better defined with continued etching, exhibiting a steeper boundary which is more pronounced with larger fluence. With prolonged etching more abrupt features with edges perpendicular to the surface are produced using high-fluence irradiation.[26]

The reflectivity spectra in Fig. 2 were recorded from MCs produced by irradiating 3×3 mm^2 areas with different proton fluences. They comprise two sequences of 12 alternating porosity bilayers, etched at 40 and 73 mA/cm^2, above and below a central layer etched at 73 mA/cm^2. The central ($\lambda/2$) layer is twice as thick as the individual ($\lambda/4$) layers of the distributed Bragg reflectors. While not considered further here it is noted that the central dip in MC reflectivity is maintained for fluences up to $1 \times 10^{15}/cm^2$ then disappears for larger fluences. Figure 3(a) shows the reflected peak λ and $\Delta\lambda$ versus fluence based on Fig. 2. For the unirradiated wafer $\lambda=740$ nm, which has blueshifted to $\lambda=490$ nm for a fluence of $2 \times 10^{15}/cm^2$. While both quantities reduce with fluence, $\Delta\lambda$ reduces notably faster.
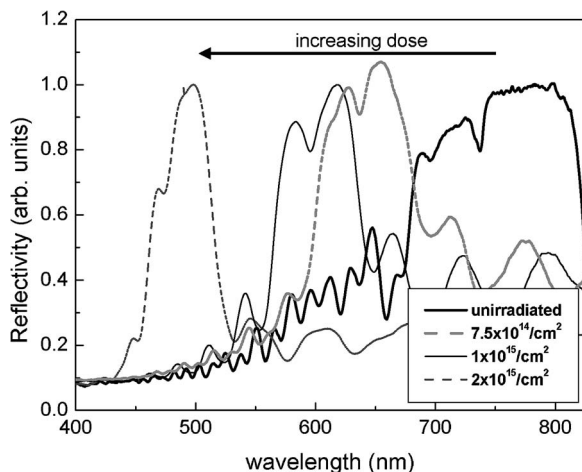
FIG. 2. Reflectivity spectra of MCs fabricated with different proton fluences. The height of each spectra is normalized to a maximum of 1.0.
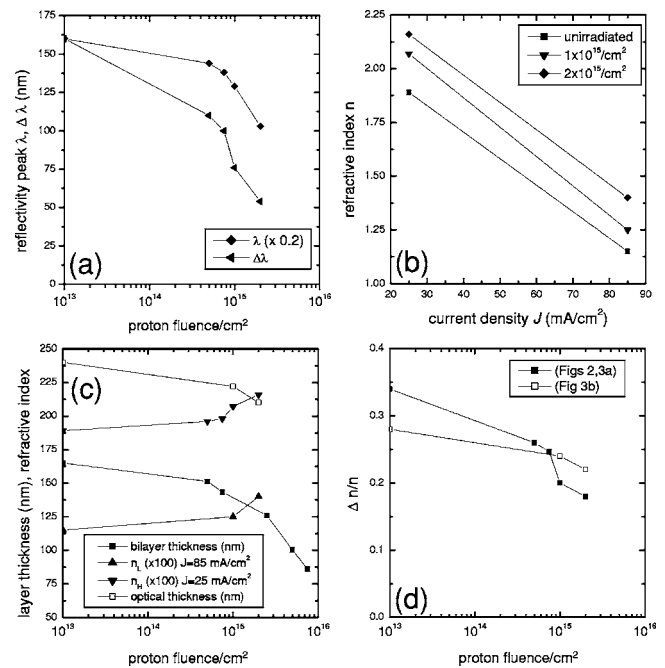
FIG. 3. (a) Variation of λ and $\Delta\lambda$ vs fluence. Values of λ are multiplied by 0.2 to normalize the unirradiated result to that of $\Delta\lambda$ for comparison of their relative rates of change. In (a), (c), and (d) the relevant value for the unirradiated wafer is that shown for a fluence of $1 \times 10^{13}/cm^2$. (b) n vs J for an unirradiated wafer and for fluences of 1×10^{15} and $2 \times 10^{15}/cm^2$. (c) Average thickness of an etched bilayer period from Fig. 1. Also shown are n_H and n_L ($\times 100$) and the average optical bilayer thickness vs fluence. (d) Ratio $\Delta n/n$.

Figure 3(b) shows n measured at 600 nm in an unirradiated wafer, and also from 3×3 mm^2 areas irradiated with fluences of 1×10^{15} and $2 \times 10^{15}/cm^2$. In each case single porous layers were separately etched at 25 and 85 mA/cm^2, producing single layers with high and low refractive indices, n_H and n_L, respectively. Over this range of fluences, the difference in refractive index, $\Delta n=n_H-n_L$, versus J is similar in the irradiated and unirradiated materials, though the average value of refractive index $\bar{n}=(n_H+n_L)/2$ increases with fluence.

Figure 3(c) shows the measured thickness of a single porous bilayer versus fluence based on Fig. 1. The measured values of n with fluence are also plotted for both 25 and 85 mA/cm^2 [same data as Fig. 3(b)]. The average optical bilayer thickness versus fluence is also shown, determined by multiplying the measured bilayer thickness with $\bar{n}$. The average optical thickness reduces with fluence because the reduction in layer thickness outweighs the increased $\bar{n}$, hence λ is blueshifted in Figs. 2 and 3(a).

The width and central wavelength of the reflected resonant peak from a distributed Bragg reflector are related to the layer refractive indices by

$$\frac{\Delta\lambda}{\lambda} \approx \frac{2}{\pi}\frac{\Delta n}{\bar{n}}. \tag{1}$$

Figure 3(b) shows that $\Delta n/\bar{n}$ is less at irradiated than unirradiated regions because $\bar{n}$ increases with fluence. Since $\Delta n/\bar{n}$ decreases with fluence then so does $\Delta\lambda/\lambda$ in Figs. 2 and 3(a) according in Eq. (1). Figure 3(d) compares $\Delta n/\bar{n}$ determined by applying Eq. (1) to the measured values of $\Delta\lambda$ and λ from Figs. 2 and 3(a), with the value obtained from Fig. 3(b). The two curves show a similar trend, which explains why the
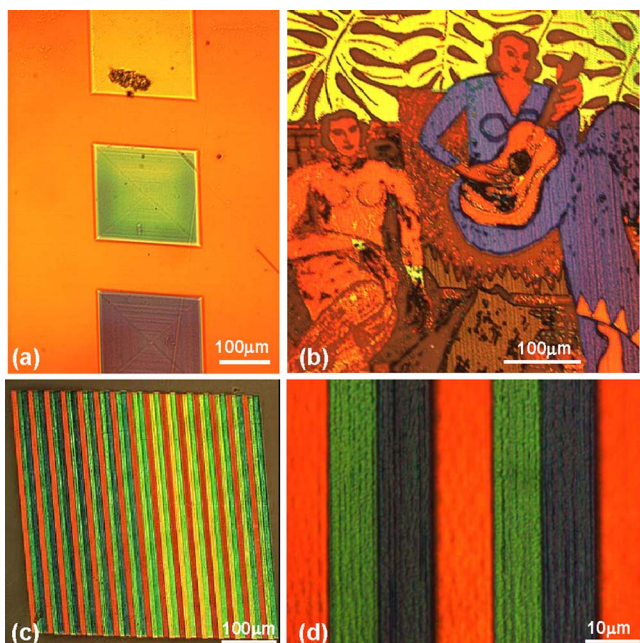
FIG. 4. (Color online) Optical reflection images of (a) 200×200 μm^2 irradiated squares. (b) Optical reflection images of the painting "La Musique" by Henri Matisse (1939), created by irradiating a 500×500 μm^2 area. [(c) and (d)] Different magnifications of vertical lines, each 10 μm wide, irradiated to form alternating red-green-blue stripes. In each recorded image the sample was illuminated with white light and the reflected light was recorded for 30 s using a Nikkon Eclipse ME600 microscope with a $\times 10$ objective.

reflectivity peak in Fig. 2 becomes so much narrower with fluence. Better agreement may be limited by refractive index measurements which are recorded from large area irradiations comprising variations in doping density or fluence, as discussed below.

Figure 4(a) shows an optical micrograph of a wafer containing three areas irradiated with increasing fluences from top to bottom. The wafer was etched at 25 and 75 mA/cm² with 12 bilayers formed in each distributed Bragg reflector above and below the central porous layer (λ in thickness) etched at 85 mA/cm². The etching period for each layer was determined by defining the central wavelength in the unirradiated regions to be $\lambda \sim 750$ nm. A range of colors is produced which are progressively blueshifted with increasing fluence. Figure 4(b) shows a more spectacular example of the ability to controllably pattern the wavelength of light which is reflected from small, adjacent regions. A 500×500 μm^2 region was irradiated with different overlaid scan patterns, with fluences from 4×10^{14} to 1.5×10^{15}/cm². The wafer was etched as in Fig. 4(a) except the etching period for each layer was chosen to give the central wavelength of $\lambda \sim 850$ nm in the unirradiated regions. Each fluence produces a different reflected color when illuminated with white light, with red/orange colors corresponding to areas irradiated with the lowest fluence. The potential of this approach to form patterned array of color pixel and lines for display applications is shown in Figs. 4(c) and 4(d), where vertical lines, each 10 μm wide, were irradiated to form alternating red-

green-blue stripes. The lateral resolution in the image is about 1 μm. Small variations in the etch current density across the region shown in Fig. 4(c) produce a shift in color across this area, which is not noticeable in the higher magnification image in Fig. 4(d).

In conclusion high-energy focused proton beam irradiation has been used to controllably blueshift the resonant wavelength of porous silicon microcavities in heavily doped *p*-type wafers. Wafers were selectively patterned to produce laterally resolved microcavities tuned to different resonant reflected wavelengths, giving rise to high-resolution full-color reflection images over the full visible spectrum. Irradiated regions are thinner and of a higher refractive index than unirradiated regions, and the microcavity blueshift arises from a net reduction in the optical thickness of each porous layer. This demonstrates the possibility of using PSi based photonic structures to selectively reflect/transmit particular wavelengths with micrometer lateral resolution for communications and display applications.

[1] L. T. Canham, Appl. Phys. Lett. **57**, 1046 (1990).
[2] O. Bisi, S. Ossicini, and L. Pavesi, Surf. Sci. Rep. **38**, 1 (2000).
[3] V. Lehmann, *Electrochemistry of Silicon* (Wiley-VCH, Weinheim, Germany, 2002).
[4] M. G. Berger, R. Arens-Fischer, M. Kruger, S. Billat, H. Luth, S. Hillbrich, W. Theiß, and P. Grosse, Thin Solid Films **297**, 137 (1997).
[5] M. Araki, H. Koyama, and N. Koshida, Appl. Phys. Lett. **69**, 2956 (1996).
[6] L. Pavesi, Riv. Nuovo Cimento **20**, 1 (1997).
[7] S. Nagata, C. Domoto, T. Nishimura, and K. Iwameji, Appl. Phys. Lett. **72**, 2945 (1998).
[8] A. Birner, R. B. Wehrspohn, U. Gösele, and K. Busch, Adv. Mater. (Weinheim, Ger.) **13**, 377 (2001).
[9] N. Savage, IEEE Spectrum **39**, 32 (2002).
[10] L. Pavesi, C. Mazzoleni, A. Tredicucci, and V. Pellegrini, Appl. Phys. Lett. **67**, 3280 (1995).
[11] C. Mazzoleni and L. Pavesi, Appl. Phys. Lett. **67**, 2983 (1995).
[12] G. Vincent, Appl. Phys. Lett. **64**, 2367 (1994).
[13] P. Ferrand, D. Loi, and R. Romestain, Appl. Phys. Lett. **79**, 3017 (2001).
[14] V. Pellegrini, A. Tredicucci, C. Mazzoleni, and L. Pavesi, Phys. Rev. B **52**, 14328 (1995).
[15] M. Cazzanelli and L. Pavesi, Phys. Rev. B **56**, 15264 (1997).
[16] S. Chan and P. M. Fauchet, Opt. Mater. (Amsterdam, Neth.) **17**, 21 (2001).
[17] P. J. Reece, G. Lerondel, W. H. Zheng, and M. Gal, Appl. Phys. Lett. **81**, 4895 (2002).
[18] M. Ghulinyan, C. J. Oton, G. Bonetti, Z. Gaburro, and L. Pavesi, J. Appl. Phys. **93**, 9724 (2003).
[19] S. Chan and P. M. Fauchet, Appl. Phys. Lett. **75**, 274 (1999).
[20] S. M. Weiss, H. Ouyang, J. Zhang, and P. M. Fauchet, Opt. Express **13**, 1090 (2005).
[21] M. B. H. Breese, D. N. Jamieson, and P. J. C. King, *Materials Analysis Using a Nuclear Microprobe* (Wiley, New York, 1996).
[22] E. J. Teo, D. Mangaiyarkarasi, M. B. H. Breese, A. A. Bettiol, and D. J. Blackwood, Appl. Phys. Lett. **85**, 4370 (2004).
[23] D. Mangaiyarkarasi, E. J. Teo, M. B. H. Breese, A. A. Bettiol, and D. J. Blackwood, J. Electrochem. Soc. **152**, D173 (2005).
[24] E. J. Teo, M. B. H. Breese, A. A. Bettiol, D. Mangaiyarkarasi, F. J. T. Champeaux, F. Watt, and D. J. Blackwood, Adv. Mater. (Weinheim, Ger.) **18**, 51 (2006).
[25] M. B. H. Breese, F. J. T. Champeaux, E. J. Teo, A. A. Bettiol, and D. J. Blackwood, Phys. Rev. B **73**, 035428 (2006).
[26] E. J. Teo, M. B. H. Breese, E. P. Tavernier, A. A. Bettiol, F. Watt, M. H. Liu, and D. J. Blackwood, Appl. Phys. Lett. **84**, 3202 (2004).